Optical Transmitter Equalization With Tunable Mismatched Terminations in a Silicon Modulator

Hector Andrade, *Member, IEEE*, Junqian Liu, *Graduate Student Member, IEEE*, Takako Hirokawa, Aaron Maharry, Ghazal Movaghar, Luis Valenzuela, *Member, IEEE*, Clint Schow, *Fellow, IEEE*, and James Buckwalter, *Fellow, IEEE*

***Abstract*— We demonstrate a 2.5 mm silicon photonics traveling-wave Mach-Zehnder modulator with on-chip tunable termination to study termination mismatching as a technique for optimizing modulator performance by leveraging the monolithic integration of electronic and photonic devices. Time domain reflectometry measurements demonstrate the tunability of the termination impedance with respect to the modulator transmission line Z_0. Electro-optic frequency response measurements show the bandwidth enhancement effect of the termination mismatch, whereby a 3 dB bandwidth above 40 GHz was achieved. Optical link time-domain measurements were performed to optimize the termination mismatch for maximum eye-diagram opening at 50 Gb/s. Our measurements demonstrate that active on-chip termination can be utilized to optimize the modulator performance and mitigate the risk incurred from fabrication variations which can result in a sub-optimal termination impedance.**

***Index Terms*— Mach-Zehnder modulator, silicon photonics, silicon modulator, fabrication variation, optical interconnect, termination mismatch.**

I. Introduction

TRAVELING-WAVE, Mach-Zehnder modulators (TW-MZMs) are widely employed in optical communications because of the inherent broadband optical response and temperature insensitivity compared to ring-resonator modulators and lower power consumption than segmented MZMs [1]. The potential of silicon photonics (SiPh) for low-cost mass production has driven considerable research interest in SiPh TW-MZMs [2], [3]. As fiber optic link bit rates continue to increase, higher bandwidth SiPh TW-MZMs will be required. For a given TW-MZM electrode and PN junction phase shifter design, the electro-optic (EO) bandwidth of the TW-MZM can be increased by using shorter length TW-MZM arms. However, this design choice increases the modulation loss, and can significantly hinder the optical link power budget. Electronic-photonic monolithic SiPh processes enable the codesign of photonic devices and active circuits and eliminate parasitic capacitances and inductances such as a wirebond inductances. Consequently, mismatched TW-MZM terminations can be explored as a bandwidth enhancement technique for the optical link.

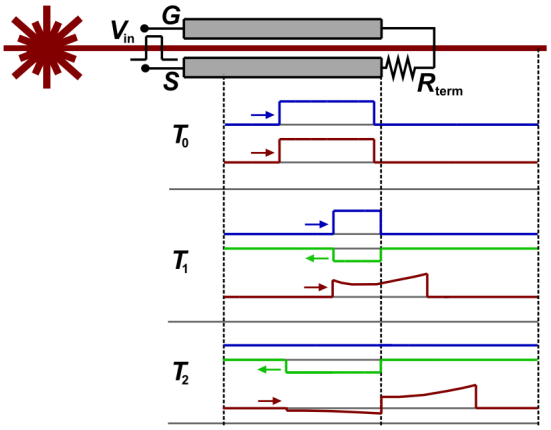

Fig. 1. Conceptual illustration of the EO pulse response of one arm of a TW-MZM in which the electrode and optical waveguide are lossless and dispersionless, and the group velocities of the optical and electrical waveforms are matched. The electrical signals and optical signals are plotted in arbitrary units of voltage and phase, respectively.

TW-MZMs are commonly terminated with a resistance (R_{term}) that matches the electrode characteristic impedance Z_0 so that the incident electrical wave is absorbed, and minimal inter-symbol interference (ISI) is generated, as no reflected electrical wave will interact with the incoming forward propagating optical wave that corresponds to the following symbols. However, termination mismatch can have a beneficial effect when $R_{term} < |Z_0|$, since a negative real reflection coefficient (Γ) produces phase-inverted reflected waves. This mechanism can be understood by visualizing the EO single-bit pulse response of one arm of a TW-MZM in which the electrode and optical waveguide are lossless and dispersionless, and the group velocities of the optical and electrical waveforms are matched. A conceptual illustration of the pulse response is shown in Fig. 1, in which the electrical and optical signals in a TW-MZM arm are plotted sequentially in three instants ($T_0 < T_1 < T_2$). In a TW-MZM, the optical phase change

Manuscript received 22 March 2022; revised 20 May 2022; accepted 18 June 2022. Date of publication 24 June 2022; date of current version 8 July 2022. This work was supported in part by the Advanced Research Projects Agency-Energy (ARPA-E), U.S. Department of Energy, under Award DEAR0000848. The views and opinions of authors expressed herein do not necessarily state or reflect those of the United States Government or any agency thereof. *(Corresponding author: Hector Andrade.)*

Hector Andrade, Junqian Liu, Aaron Maharry, Ghazal Movaghar, Luis Valenzuela, Clint Schow, and James Buckwalter are with the Department of Electrical and Computer Engineering, University of California Santa Barbara, CA 93106 USA (e-mail: handrade@ucsb.edu).

Takako Hirokawa is with GlobalFoundries, Santa Clara, CA 95054 USA.

Color versions of one or more figures in this letter are available at https://doi.org/10.1109/LPT.2022.3186237.

Digital Object Identifier 10.1109/LPT.2022.3186237

induced by the electrical signals is integrated with respect to time, therefore the effect of the termination mismatch corresponds to the integrals across the time intervals $T_0 - T_1$ and $T_1 - T_2$. The electrical signals are plotted in arbitrary units of voltage, and the optical signal is plotted in arbitrary units of phase. At T_0 the forward-traveling electrical pulse (FTEP, depicted in blue) and forward-traveling optical pulse (FTOP, depicted in red) are propagating along the TW-MZM arm alongside at the same velocity. As the leading edge of the FTEP arrives at the end of the electrode, an inverted backwards-traveling electrical pulse (BTEP, depicted in green) starts to propagate. At T_1 the end of the FTEP is still propagating along the arm, while the front part of the FTEP has been partially absorbed by the R_{term} and partially reflected back to generate the BTEP. The sum of the FTEP and BTEP widths is therefore equal to the initial FTEP width prior to reaching the end of the electrode. The BTEP produces a phase change in the FTOP that is opposite to the one produced by the FTEP. In this example, the leading edge of the FTOP does not interact with the BTEP and the accumulated FTOP phase shift from the BTEP is largest near the trailing edge of the FTOP. In the time domain, this results in a modulated signal with emphasis at the bit transitions, as depicted in T_1. In the frequency response, this introduces peaking at high frequencies by de-emphasizing the low-frequency content of the signal. At T_2 the trailing edge of the FTEP has reached the end of the electrode and the BTEP has interacted with the continuous-wave optical carrier. Since the pulse width corresponds to one bit period, this interaction produces ISI. However, in a bandwidth limited optical link, the impact of the peaking effect due to the reflections can reduce the overall ISI.

In this work, we implemented a SiPh TW-MZM with tunable termination to study the effect of the mismatch on the performance of an optical link. NRZ eye diagrams at 50 Gb/s were obtained and a method for full-optical link optimization based on termination mismatch tuning is demonstrated.

II. Circuit Schematic and Simulations

Fig. 2 depicts the schematic and small signal model of one of the two arms of the TW-MZM with the tunable termination circuit. The PN junction optical phase shifter extends from the signal electrode to one of the two ground electrodes. The tunable termination between the signal electrode and each adjacent ground electrode consists of an NFET in series with a 50 Ω resistor (R_2). A parallel branch of 8 kΩ resistors (R_1) provides ESD protection at the NFET gate. The termination impedance (Z_{term}) is determined by V_{res}, which sets the NFET V_{gs}. The gate shunt resistor (R_g) is 2 kΩ. The small-signal model, accounting only for the gate-source capacitance, indicates that R_g produces an inductive response in Z_{term} that can be tuned with V_{res}. At high frequency, $Z_{in} \approx R_g$, and at low frequency $Z_{in} \approx 1/g_m$, assuming $R_g \gg 1/g_m$. As a result of the inductive response, the termination can be tuned such that $|\Gamma|$ is larger at lower frequency, which further emphasizes the high frequency content of the EO response.

The simulated Z_{term} vs frequency at various V_{res} values and a fixed V_{PN} of −1.8 V is shown in Fig. 3 (a). As V_{res} increases, the g_m decreases, which reduces the inductive response of the termination. Due to the inductive response, the Z_{term} initially increases with frequency. However, beyond 20 GHz, the Z_{term} decreases with frequency due to additional parasitic capacitances. The simulated low frequency Z_{term} vs V_{PN} and V_{res} is shown in Fig. 3 (b).

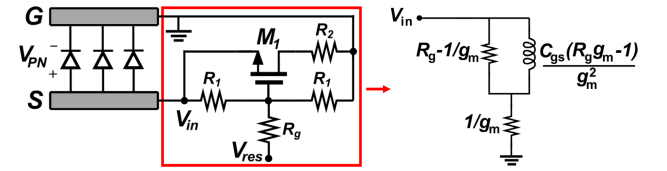

Fig. 2. Schematic and small signal model of one of the two arms of the TW-MZM with the tunable termination circuit.

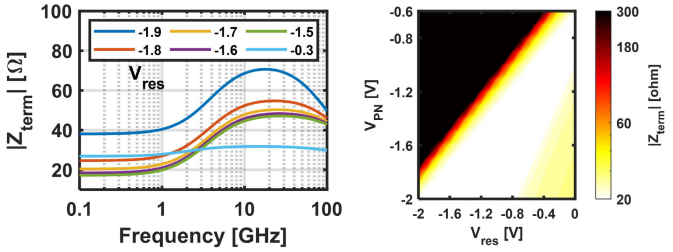

Fig. 3. (a) Simulated Z_{term} vs frequency at various V_{res} values, at $V_{PN} = -1.8$ V. (b) Simulated low frequency Z_{term} vs V_{PN} and V_{res}.

III. Experimental Results

A. Fabrication and Assembly

A SiPh O-band TW-MZM with a tunable termination was fabricated in the GlobalFoundries 9WG 90-nm CMOS electronic-photonic monolithic process. The die micrograph is shown in Fig. 4 (a). The CPW transmission line electrodes have a GSGSG configuration. The electrode widths are 2 μm, 172 μm, and 100 μm for the signal and grounds, respectively. The high-frequency phase shifters are based on the plasma dispersion effect. The $V_\pi L$ is 15 V*cm at 2 V reverse bias and the low phase efficiency is due to a modification in the fabrication process. Vertical grating couplers (GC) were utilized to couple light into and out of the modulator. The electrodes are 2.5 mm long, and the TW-MZM device including the tunable termination has a lengh of 3.5 mm. The wirebonded TW-MZM assembly is shown in Fig. 4 (b). The PCB packaging platform used is described in [4]. Fig. 4 (c) shows the RF cables and mini-SMP connectors used to drive the modulator differentially and the vertically-coupled input/output fibers.

B. Time Domain Reflectometry Measurements

Time domain reflectometry (TDR) measurements were done on the TW-MZM at various PN junction biases and V_{res} values. Fig. 5 (a) shows single-ended TDR data for various V_{res} values at a fixed V_{PN} of −1.8 V. The 6 TDR curves are identical from 0 to 350 ps. This segment corresponds to the end of the RF cable, mini-SMP RF connector, PCB transmission line, wirebonds and the TW-MZM electrode. The effect of the tunable termination can be observed after 350 ps.

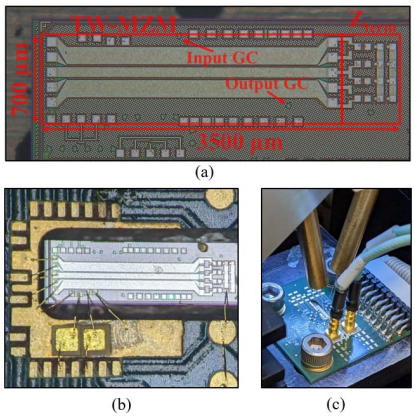

Fig. 4. (a) Micrograph of the 2.5 mm SiPh TW-MZM with tunable termination. The TW-MZM device including the tunable termination has a lengh of 3.5 mm. (b) Wirebonded TW-MZM assembly on a PCB. (c) Packaged TW-MZM with RF cables and vertically-coupled fiber.

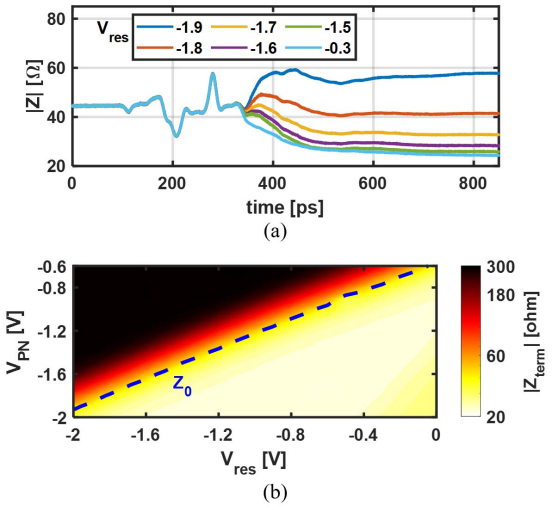

Fig. 5. (a) TDR data for various V_{res} values at a fixed V_{PN} of -1.8 V. (b) Contour plot of Z_{term} vs V_{PN} and V_{res}.

The TW-MZM Z_0 is around 45 Ω. For $V_{res} = -1.9$ V Z_{term} is significantly higher than the $Z_(0)$. As V_{res} is increased, Z_{term} decreases. For $V_{res} = -1.8$ V, the low-frequency Z_{term} is 40 Ω and it is approximately matched to the TW-MZM. For $V_{res} = -0.3$ V, the low-frequency Z_{term} is 23 Ω. The response becomes less inductive with higher V_{gs}, in agreement with the small-signal model and the simulated $Z_{in}(f)$. Fig. 5 (b) shows a contour plot of Z_{term} vs V_{PN} and V_{res}. The blue dashed line in the contour plot indicates the Z_0 at each V_{PN} value. For a V_{PN} of -1.6 V to -0.6 V, Z_{term} ranges from above to below Z_0.

C. Frequency Response Measurements

A Keysight PNA-X 67 GHz network analyzer with a lightwave component analyzer (LCA) was used to characterize the effect of the tunable termination on the EO frequency response. Fig. 6 (a) contains the measured EO frequency response of the TW-MZM for the same V_{PN} and V_{res} values

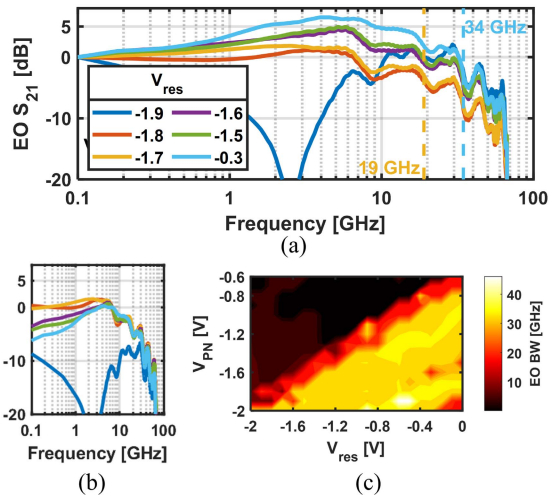

Fig. 6. (a) Measured EO frequency response of the TW-MZM for $V_{PN} = -1.8$ V at various V_{res} values. (b) Un-normalized frequency response. (c) Contour plot of the 3 dB EO BW vs V_{res} and V_{PN}.

plotted in Fig. 5 (a). The curves are smoothed using an 11-point moving average filter to mitigate the effect of optical reflections in the setup. A reduction in Z_{term} impacts the transmitter gain since the driver voltage swing is proportional to the parallel driver load resistance given by $R_D = 50\Omega || R_{term}$. The curves are normalized to 0 dB at low-frequency. For $V_{res} = -1.9$ V, $Z_{term} > Z_0$, so the Γ is positive, and the detrimental effect results in a BW of 300 MHz. As V_{res} is increased to -1.7 V, the BW increases to 19 GHz. At $V_{res} = -0.3$ V the Z_{term} mismatch is maximized, and the BW increases to 34 GHz. Fig. 6 (b) shows the un-normalized responses to demonstrate how the EO BW is enhanced by de-emphasizing the low-frequency response. In addition to the effect of the Z_{term}, the un-normalized curves also capture variations in coupling losses due to vibrations in the test setup. Fig. 6 (c) contains a contour plot of the 3 dB EO BW vs V_{res} and V_{PN}, which denotes the trend, across the entire V_{PN} range, of BW enhancement as Z_{term} decreases.

D. Mismatch Optimization and Time Domain Measurements

The time-domain measurement setup is shown in Fig. 7. A Centellax 50 Ω 4.5 V_{pp} driver and a Finisar receiver rated for 43 Gb/s with integrated limiting amplifiers were used to obtain the time-domain response of the full optical link. An SHF bit-pattern generator (BPG) was used to generate a PRBS7 400 mV_{pp} at the driver input and the receiver output was measured using a Tektronix sampling oscilloscope (SO). Bias tees were used to reverse bias the PN junction phase shifters of the TW-MZM. The signal was averaged 500 times in the SO by triggering on each PRBS7 word to reduce the effects of random noise on eye closure. This improves the SNR by 27 dB. In addition to improving the SO sensitivity to mitigate the effects of the low TW-MZM phase efficiency, the ISI of the eye is characterized.

Normalized vertical and horizontal eye openings at 50 Gb/s as a function of V_{PN} and V_{res} are shown in Fig. 8.

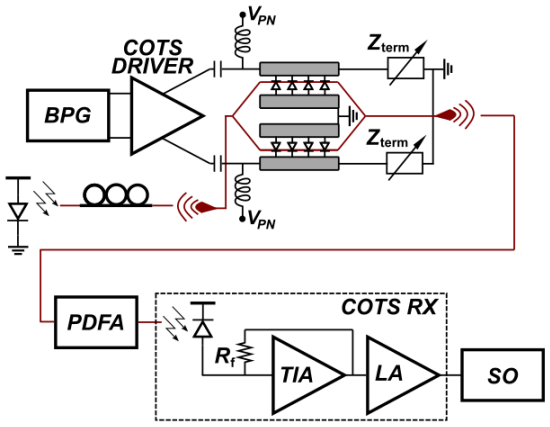

Fig. 7. Time-domain measurement setup using a commercial driver and receiver.

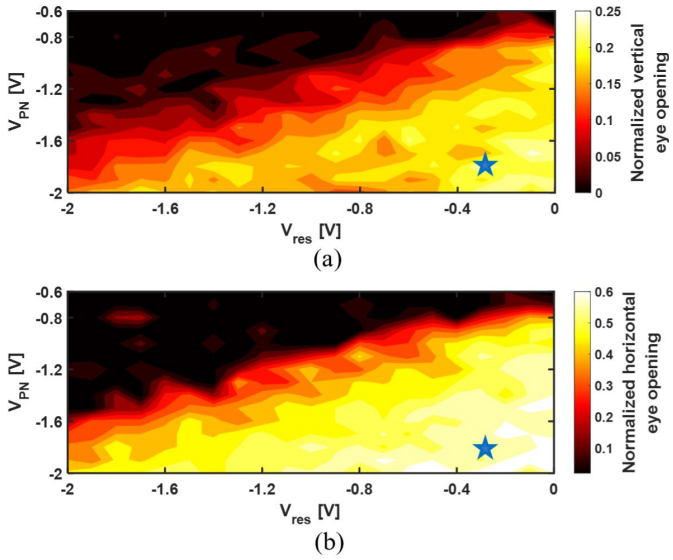

Fig. 8. Normalized vertical and horizontal eye openings at 50 Gb/s as a function of V_{PN} and V_{res}. The blue markers denote the setting with the largest vertical eye opening.

The contour plots demonstrate the optimal vertical and horizontal eye openings occur with lower Z_{term}. While Fig. 6 (c) shows a maximum EO BW $>$ 40 GHz, the optimal setting in terms of eye-opening is at 34 GHz BW. The blue markers denote the setting with the largest vertical eye opening: $V_{PN} = -1.8$ V and $V_{res} = -0.3$ V, for which $Z_{term} = 23\ \Omega$ and EO BW = 34 GHz. Compared to a matched 45 Ω termination, the reduced voltage swing for a 50 Ω driver results in a 3.3 dB penalty on the optical link. This modulation penalty is offset by the ISI penalty reduction due to BW enhancement. The power dissipation also increases, as it is inversely proportional to R_{term}. The power can be significantly reduced by enabling only differential termination for which no path to DC ground is required.

Fig. 9 contains the pattern-averaged PRBS7 eye-diagrams at 50 Gb/s. To characterize the commercial receiver, an optical eye diagram from the Fujitsu MZM was obtained using an optical sampling module (Fig. 9 (a)) and the corresponding

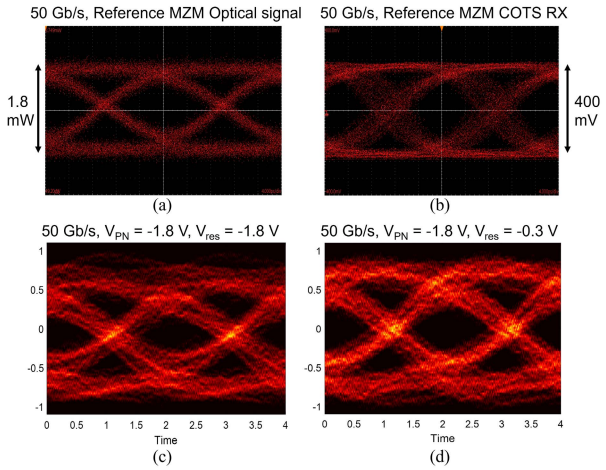

Fig. 9. Measured PRBS7 eye-diagrams at 50 Gb/s. (a) Reference MZM measured with the SO optical module. (b) Reference MZM measured with the COTS RX and SO electrical module. (c) and (d) are of the TW-MZM measured with the COTS RX and SO electrical module with different tunable termination settings.

electrical eye diagram was measured at the output of the Finisar receiver (Fig. 9 (b)), which shows the effect on eye closure produced by the receiver response. Eye diagrams for $V_{PN} = -1.8$ V, $V_{res} = -1.8$ V and $V_{PN} = -1.8$ V, $V_{res} = -0.3$ V, shown in Fig. 9 (c) and (d), respectively, demonstrate the improvement that results from optimizing the termination mismatch.

IV. Conclusion

This work demonstrates that an on-chip tunable mismatched termination can produce desirable equalization in an electronic-photonic monolithic process. The equalization is achieved by de-emphasizing the low-frequency response and not by amplifying the high-frequency response. In TW-MZMs with passive resistor termination, process variations can result in a sub-optimal Γ, which can severely hinder EO performance. Furthermore, eye diagram measurements demonstrate that optimizing termination mismatch minimizes the overall ISI. The optimal mismatch configuration depends on the receiver characteristics. For these reasons, it can be advantageous to have termination tunability.

Acknowledgment

The authors would like to thank GlobalFoundries for their support and assistance.

References

[1] J. Witzens, "High-speed silicon photonics modulators," *Proc. IEEE*, vol. 106, no. 12, pp. 2158–2182, Dec. 2018.
[2] J. Zhou, J. Wang, L. Zhu, and Q. Zhang, "Silicon photonics for 100Gbaud," *J. Lightw. Technol.*, vol. 39, no. 4, pp. 857–867, Feb. 15, 2021.
[3] P. Absil *et al.*, "Reliable 50 Gb/s silicon photonics platform for next-generation data center optical interconnects," in *IEDM Tech. Dig.*, Dec. 2017, p. 34.
[4] A. Maharry, L. A. Valenzuela, J. F. Buckwalter, and C. L. Schow, "A PCB packaging platform enabling 100+ Gbaud optoelectronic device testing," in *Proc. IEEE 71st Electron. Compon. Technol. Conf. (ECTC)*, Jun. 2021, pp. 1323–1328.